Nanoscale

Aromatic carbohydrate amphiphile disrupts cancer spheroids and prevents relapse

Journal:	*Nanoscale*
Manuscript ID	NR-COM-07-2020-005008.R1
Article Type:	Communication
Date Submitted by the Author:	n/a
Complete List of Authors:	Brito, Alexandra; University of Minho, 3B's Research Group; ICVS/3B's - PT Government Associate Laboratory, Pereira, Patrícia; Memorial Sloan Kettering Cancer Center, Department of Radiology Reis, Rui; University of Minho School of Engineering Ulijn, Rein; CUNY Advanced Science Research Center, ; The University of Strathclyde, Department of Chemistry/ WestCHEM Lewis, Jason; Memorial Sloan-Kettering Cancer Center, Radiology Pires, Ricardo; University of Minho, 3Bs Research Group, I3Bs – Research Institute on Biomaterials, Biodegradables and Biomimetics University of Minho, Headquarters of the European Institute of Excellence on Tissue Engineering and Regenerative Medicine. Pashkuleva, Iva; University of Minho, 3B's Research Group

Nanoscale

Guidelines for Referees

Thank you very much for agreeing to review this manuscript for *Nanoscale*.

Nanoscale is a high impact international journal, publishing high quality research across nanoscience and nanotechnology. It publishes a full mix of research articles on experimental and theoretical work, including reviews, communications and full papers.

Nanoscale Associate Editors stress very high standards for acceptance in the journal. Articles must report extremely novel, very high quality, reproducible new work of broad general interest.

Nanoscale's Impact Factor is **6.970** (2018 Journal Citation Reports®)

The following manuscript has been submitted for consideration as an

COMMUNICATION

Articles should be contain either a complete study or a preliminary report, but in either case must present an important advance of immediate interest to the *Nanoscale* readership in the field of nanoscience and nanotechnology. Communications will not normally exceed the length of 4 printed journal pages, however, exceptions may be made at the editor's discretion.

When preparing your report, please:

- Focus on the **originality**, **importance**, **impact** and **reproducibility** of the science.
- Refer to the **journal scope and expectations**.
- **State clearly** whether you think the article should be accepted or rejected and give detailed comments (with references) both to help the Editor to make a decision on the paper and the authors to improve it
- **Inform the Editor** if there is a conflict of interest, a significant part of the work you cannot review with confidence or if parts of the work have previously been published.
- **Provide your report rapidly** or inform the Editor if you are unable to do so.

Best regards,

Professor Chunli Bai
Editor-in-Chief, *Nanoscale*

Professor Dirk Guldi
Editor-in-Chief, *Nanoscale*

Dr Michaela Muehlberg
Managing Editor, *Nanoscale*

Contact us

Please visit our reviewer hub for further details of our processes, policies and reviewer responsibilities as well as guidance on how to review, or click the links below.

What to do when you review

Reviewer responsibilities

Process & policies

COMMUNICATION

Aromatic carbohydrate amphiphile disrupts cancer spheroids and prevents relapse

Received 00th January 20xx,
Accepted 00th January 20xx

DOI: 10.1039/x0xx00000x

Alexandra Brito,[a-d] Patrícia M. R. Pereira,[c] Rui L. Reis,[a,b] Rein V. Ulijn,[d-f] Jason S. Lewis,[c,g-j] Ricardo A. Pires*[a,b] and Iva Pashkuleva *[a,b]

Spheroids recapitulate the organization, heterogeneity and microenvironment of solid tumors. Herein, we targeted spatiotemporally the accelerated metabolism of proliferative cells located on the spheroid surface that ensure structure maintenance and/or growth. We demonstrate that phosphorylated carbohydrate amphiphile acts as a potent antimetabolite due to glycolysis inhibition and to *in situ* formation of supramolecular net around spheroid surface where alkaline phosphatase is overexpressed. The efficiency of the treatment is higher in spheroids as compared to the conventional 2D cultures because of the 2-fold higher expression of glucose transporter 1 (GLUT1). Moreover, treated spheroids do not undergo following relapse.

Biocatalytic self-assembly (BSA) combines the selectivity of an enzymatic conversion with the sensitivity and the precision of the supramolecular self-assembly.[1, 2] The approach has been applied to different pathologies, including cancers, where an overexpressed enzyme triggers *in situ* fiber formation by localized self-assembly leading to cell death or localized drug delivery through triggered disassembly of designed precursors.[1-6] BSA efficiency and *modus operandi* are usually demonstrated *in vitro* using two-dimensional (2D) cell cultures.[4, 7-9] While these cultures serve as suitable proof-of-concept model systems because of the high reproducibility and ease of handling, they do not recapitulate the complex tumor microenvironment: tumors are heterogeneous and complex organ-like structures, whose identity is dependent on the cell-to-cell contacts and alterations of the extracellular matrix.[10, 11] These characteristics are particularly relevant in BSA, where proteins present at the cell membrane are used as a trigger of the self-assembly process.

Herein, we developed a 3D tumor model using HS578T human breast cancer cells and studied BSA of the phosphorylated carbohydrate amphiphile, N-fluorenylmethyloxycarbonyl-glucosamine-6-phosphate (**1**). This amphiphile can be transformed by alkaline phosphatase (ALP) overexpressed in some tumors, *e.g.* osteosarcoma, into the low molecular mass gelator N-fluorenylmethyloxycarbonyl-glucosamine (**2**) that self-assembles into a nanoscale network (Scheme 1c) which sequesters and efficiently kills cancer cells.[4]

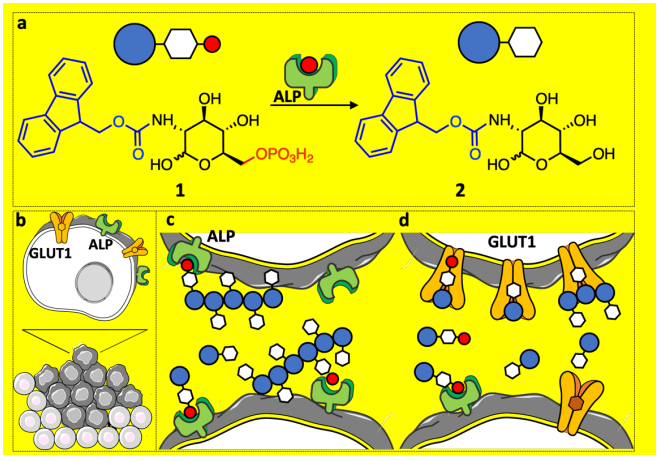

Scheme 1. (a) Schematic presentation of the enzymatic transformation of the phosphorylated precursor **1** to carbohydrate amphiphile **2**. **(b-d)** In tumors this transformation can trigger **(c)** self-assembly on the tumor surface and **(d)** blocking of the GLUT1 expressed by the proliferative cells on the tumor surface.

[a] *3B's Research Group, I3Bs - Research Institute on Biomaterials, Biodegradables and Biomimetics, University of Minho, Headquarters of the European Institute of Excellence on Tissue Engineering and Regenerative Medicine, AvePark, Parque de Ciência e Tecnologia, Zona Industrial da Gandra, 4805-017 Barco, Guimarães, Portugal*
[b] *ICVS/3Bs - PT Government Associate Laboratory, Braga/Guimarães, Portugal*
[c] *Department of Radiology, Memorial Sloan Kettering Cancer Center*
[d] *Advanced Science Research Center (ASRC) at the Graduate Center, City University of New York (CUNY), 85 St Nicholas Terrace, New York, New York 10031, USA*
[e] *Department of Chemistry, Hunter College, City University of New York, 695 Park Avenue, New York 10065, USA*
[f] *PhD programs in Biochemistry and Chemistry, The Graduate Center of the City University of New York, New York 10016, USA*
[g] *Department of Radiology, Weill Cornell Medical College, New York, NY 10065, USA*
[h] *Molecular Pharmacology Program, Memorial Sloan Kettering Cancer Center, New York, NY 10065, USA*
[i] *Department of Pharmacology, Weill Cornell Medical College, New York, NY 10065, USA*
[j] *Radiochemistry and Molecular Imaging Probes Core, Memorial Sloan Kettering Cancer Center, New York, NY 10065, USA*
* rpires@i3bs.uminho.pt; pashkuleva@i3bs.uminho.pt
Electronic Supplementary Information (ESI) available: [details of any supplementary information available should be included here]. See DOI: 10.1039/x0xx00000x

Beyond the physical effect of creating a nanoscale network that acts as a barrier at the cell surface, there is also a specific chemical role for these glucose-based aromatic amphiphiles. The phosphorylated precursor **1** and its dephosphorylated analogue **2** contain a glucose moiety that interacts with glucose transporter 1 (GLUT1) (Scheme 1d), overexpressed in different cancers, thus, allowing double targeting, as we recently demonstrated.[12]

We have selected three cell lines for spheroid formation, namely SaOs2 osteosarcoma, HS578T breast and MCF7 breast cancer cells because they all overexpress ALP, GLUT1 and caveolin 1 (CAV1) (Figure S1).[13] Our interests in GLUT1- and ALP-overexpressing cell lines is related to the affinity of compound **1** for those proteins: **1** can bind to GLUT1 because of the glucose moiety (Scheme 1d) and can be transformed in the self-assembling **2** upon ALP action (Scheme 1c).[4, 12] In addition to GLUT1 and ALP, we also explored the contribution of CAV1 in carbohydrate amphiphile mediated BSA processes. CAV1 is the main structural protein of caveolae, the small pockets in the cell membrane that are known to modulate the glycolysis and to interact dynamically with ALP.[14, 15]

Formation of spheroids was studied by seeding the selected cell lines on agarose-coated well plates at different density (2,500-20,000 cells per well) and culture time (24 – 72 h).[11] Among the tested cells, only HS578T cells formed spheroids in a highly reproducible manner (Figures S2 and S3): 24 h after seeding, HS578T cells gathered into unstable aggregates, which were easily disrupted by mechanical force (*e.g.* pipetting). After 48 h, we observed formation of compact and stable spheroids composed by a shell of viable cells (Figure 1a) surrounding a necrotic core (Figure 1b), which is typical for solid tumors.[10] Further compacting and a significant reduction in the spheroid volume were observed in the following 24 h (Figure S3). We selected a cell density of 5,000 cells/well and 48 h of culture time for the spheroids' formation.

The structure of the spheroids (proliferative and quiescent cellular compartments) evidenced gradual deprivation of nutrients and oxygen from the surface to the bulk of the 3D structure. Such gradient is distinctive for solid tumors and is associated with specific genetic and metabolic changes. As an example, cells in the core are adapting to an anaerobic metabolism and produce large amount of lactate used as a source of energy.[16] This scenario is significantly different from 2D cultures where no competition for nutrients and oxygen exist and the population is homogeneous.

The comparison between HS578T monolayers and spheroids showed that both cultures expressed ALP, GLUT1 and CAV1 proteins (Figures 1c and S1): ALP expression in spheroids was similar to that found in monolayers but both GLUT1 and CAV1 expression were found to be substantially different from that obtained for the 2D cell culture. In accordance with previous studies, we detected 3-fold lower CAV1 expression in spheroids when compared with monolayers.[17] On the other hand, a 2-fold increase in GLUT1 expression was observed when cells were cultured in spheroids. GLUT1 expression in spheroids and solid tumors is commonly higher than in the respective 2D cultures.[11, 18-20] This overexpression is associated with the survival mechanism(s) activated by the cells in the hostile tumor environment and correlates with aggressive, metastatic behavior.[18, 19] GLUT1 is therefore both prognostic marker and therapeutic target.[21-23]

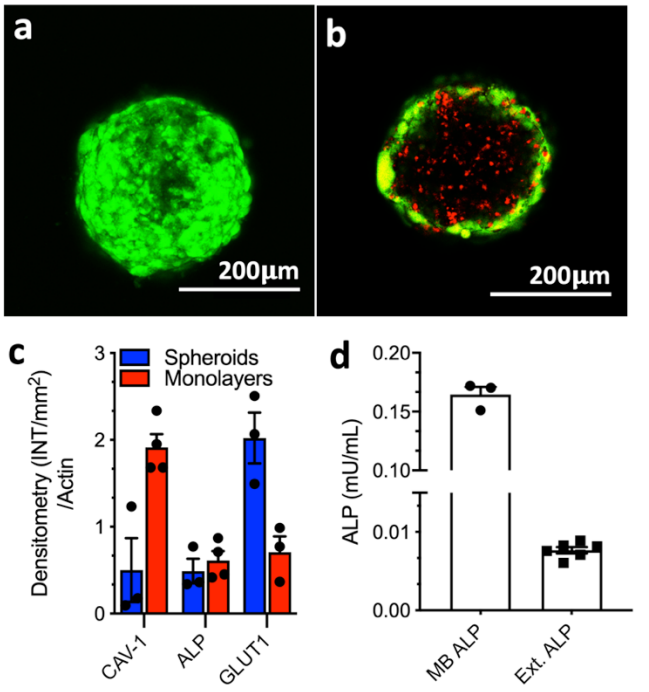

Figure 1. Characterization of the HS587T spheroids: Representative confocal microscopy images of **(a)** spheroid surface (whole spheroid projection) and **(b)** core (single focal plane/z-stack) stained for live (green, calcein AM) and dead (red, propidium iodide) cells; **(c)** Densitometry quantification of Western-Blot analysis of ALP, CAV1, and GLUT1 expression by the 3D spheroids and 2D cell culture, normalized to the total β-actin protein content; **(d)** expression of membrane-bound (MB) and extracellular (Ext.) ALP in spheroids.

Among the heterogenous cell populations within the tumors, the proliferative cells on the surface are unique because they sustain the structure growth and provide an interface between the tumor and its environment. Thus, spatiotemporal targeting of these surface cells at their proliferative phase provides a very efficient mean of isolating and destroying the tumors. The high energy demands of cancer cells especially during their proliferation instruct accelerated metabolism associated with high glucose consumption/ dependence and overexpression of GLUT1 (Warburg effect).[18, 24, 25] Therefore, we expected that the GLUT1 antagonist **1** will decelerate their metabolism crucial for tumor maintenance.[12, 21, 22] On the other hand, these surface cells are not adapted to an anaerobic metabolism and the formation of ALP catalyzed BSA nanostructured network around the tumor will affect them further by deprivation of nutrients and oxygen.[2, 4, 26]

The addition of **1** to the spheroids resulted in their partial disintegration in a concentration and time-dependent manner (Figures 2 and S4): the effect of **1** on the spheroid morphology was visible after 48 h when 0.5 mM concentration was used and this time was shortened to 24 h upon a concentration increase to 1 mM. A closer look at the spheroids revealed the formation of a nanofibrous coating on the surface of the samples treated

for 48 h, suggesting the occurrence of *in situ* BSA (Figures 2f and S8). These nanostructures were absent in the control sample. Previously, we have observed a similar effect in 2D cultures of ALP overexpressing osteosarcomas SaOs2 that showed reduced metabolic activity at shorter culture time (1-7 h), which caused cell death at longer exposure (≥ 24 h) to **1**.[4]

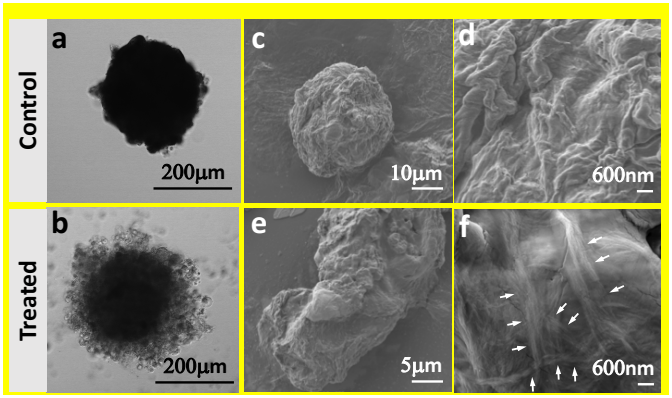

Figure 2. Effect of **1** on spheroid integrity and morphology: Representative **(a, b)** confocal microscopy and **(c-f)** high-resolution scanning electron microscopy images of untreated spheroids (control) and spheroids treated with **1** (1 mM, 48 h). White arrows indicate different fibers bundles.

The morphological differences observed for the spheroids were accompanied by an increased release of lactate dehydrogenase (LDH) in the extracellular milieu of the treated samples (Figure 3a). This increase indicates compromised or damaged plasma membrane and is commonly used as a marker of necrotic cell death.[27] Indeed, histological staining of the spheroids with hematoxylin and eosin showed typical necrotic areas formed by cells without nuclei (Figure 3e, yellow circlers).[28] Live/dead staining also corroborated a significant increment of cell death in spheroids treated with **1** (Figure 3d).

Confirmation of BSA involvement in cell death was done by quantification and inhibition of ALP that triggers the self-assembly process. We quantified both membrane-bound and extracellular ALP in the spheroids and found 20-fold higher values for the former form (Figure 1d), suggesting its involvement in the BSA. Immunolocalization of membrane-bound ALP confirmed this result: the presence of **1** increased the expression of ALP on the cell surface (Figure S5). We then studied the inhibition of ALP using pierce phosphatase inhibitor.[4] The addition of the inhibitor rescued the cells and the spheroids had a similar shape and cell viability when compared to the control spheroids (Figure 3f), manifesting a direct relationship between the ALP activity and the cytotoxicity of **1**.

Glycolysis deprivation *via* blockage of GLUT1 by **1** and **2** was also studied as an additional contributor to cell death.[12] As noted, spheroids have a higher expression of GLUT1 as compared to the 2D cell culture (Figure 1c). We knocked down GLUT1 expression in the spheroids by transfection with three target-specific siRNAs (Figure S6). Exposure of the transfected spheroids to **1** led to a reduction of the of LDH release, *i.e.* a significant decrease in the cytotoxicity of **1** (Figure 3g). This result confirms that **1** and/or its dephosphorylated analog **2** interact with GLUT1 and the observed cytotoxicity is also mediated by this interaction.

Because ALP is present within caveolae and CAV1 is involved in glycolysis,[14] we also investigated possible interactions between this protein and **1** in the spheroids (Figure S5). CAV1 protein was knocked down[29] (Figure S6) but its depletion did not affect the toxicity of **1** (Figure 3h), showing no direct participation of CAV1 in the necrotic pathway. Similar results (not shown) were obtained for 2D cultures with higher expression of CAV1.

A comparison of the effect of **1** on spheroids (Figure 3) and 2D cell culture (Figure S7) showed important differences: while cell death in 2D culture increases with increment of both the concentration of **1** and the treatment time, in the 3D spheroids we observed a maximum effect of **1** at lower concentration (*i.e.* 0.5 mM) and shorter treatment time (48 h). Further increase of the concentration of **1** (*i.e.* to 1 mM) or extension of the treatment timeframe (72 h) did not induce additional cell death in the spheroids. This result indicates that either there is a higher sensitivity of the spheroids to **1** or there is an inefficiency of the treatment at the studied conditions.

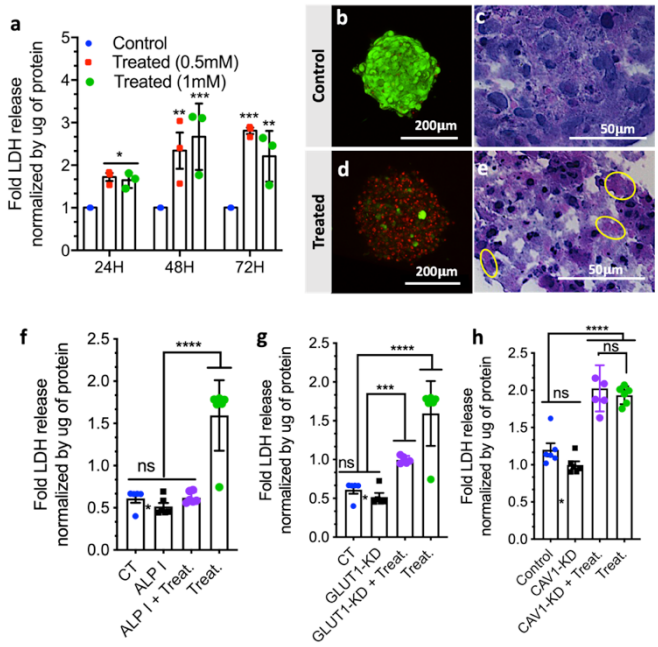

Figure 3. Effect of **1** on cell viability in HS578T spheroids: **(a)** Normalized LDH release as a function of time and concentration of 1; **(b-e)** Cell death shown by microscopy images after (**b, d**) live/dead (projection of the whole spheroid) and (**c, e**) hematoxylin/eosin staining. LDH release of HS578T spheroids as a function of **(f)** ALP inhibition (I), **(g)** GLUT1 and **(h)** CAV1 knockdown (KD). The applied treatment (Treat.) was spheroid exposition to 1 (1 mM, 48 h). Statistics: ns (non-significant); * $p < 0.01$; ** $p < 0.005$; *** $p < 0.001$; **** $p < 0.0001$.

We, therefore, studied the possibility of recovery of the remaining live cells within the treated spheroid as a forecast of clinical scenario known as a relapse. Cancer recurrence and tumor relapse (usually in a more resistant form) caused by resistant cells within the tumors is one of the major hurdles in the development of efficient anti-cancer therapies. We re-plated the treated spheroid in an adherent well plate and

confirmed that the cells were not able to recover from the effect of **1**, supporting the efficacy of the treatment (Figure 4d). When untreated spheroid was re-plated, we observed formation of a dense spheroid (Figure 4c). Because ALP expression is similar for 2D cultures and 3D spheroids (Figure 1c), we suggest that the observed higher sensitivity of the 3D tumor model to **1** is due to the GLUT1 overexpression in spheroids. Thus, the use of the GLUT1 antagonist **1** as a substrate in a BSA anticancer therapeutic approach has two advantages. The first one is the enhanced efficacy: the high malignant potential of resistant cells is related to their ability to self-renew and form prone differentiated progeny that compose the bulk of the relapsed tumor - an energy-demanding process that depends on glucose uptake. In the presence of **1**, some of these cells can survive, but their proliferative potential is significantly reduced due to the GLUT1 inhibition and deprivation of the glucose uptake. The second advantage is the selectivity: the overexpression of GLUT1 in solid tumors, and especially cells located at the surface makes it suitable target for a selective therapy.

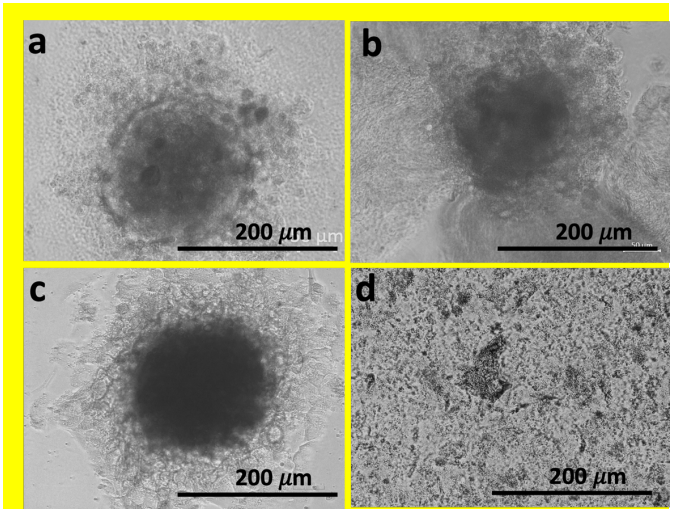

Figure 4. Spheroid relapse: representative transmitted-light microscope images of **(a)** untreated spheroid (control) and **(b)** spheroid exposed to **1** (1 mM, 48 h) that were re-plated (**c** control and **d** treated) in adherent well plates for 48 h.

In summary, we demonstrated that variable expression levels of the same proteins in 3D tumor models and 2D cell cultures can render dramatically different sensitivity to chemotherapies. We validated this observation by using carbohydrate amphiphile **1** that participates simultaneously in two processes that are sensitive to the surface expression of two proteins, namely BSA triggered by membrane-bound ALP and glycolysis inhibition by blockage of GLUT1. Our data show that the combination of supramolecular chemistry with the manipulation of vital biochemical cascades is feasible approach to achieve efficient cancer therapies.

Conflicts of interest

There are no conflicts to declare.

Acknowledgements

This work was supported by the EU's H2020 program (Forecast 668983), the Portuguese Foundation for Science and Technology (grants BD/113794/2015; PTDC/NAN-MAT/28468/2017 and PTDC/BTM-MAT/28327/2017), the US Army Research Laboratory and US Army Research Office (contract/grant W911NF-16-1-0113), NSF (grant 1808143), and the research infrastructure support of the NSF CREST Center IDEALS (grant 1547830). AB thanks to the Portuguese league against cancer for her fellowship. The authors also acknowledge the Radiochemistry and Molecular Imaging Probe Core which was supported by NIH grant P30 CA08748. This study was supported in part NIH NCI R35 CA232130 (to J.S. Lewis). P.M.R. Pereira acknowledges the Tow Foundation Postdoctoral Fellowship from the MSKCC Center for Molecular Imaging and Nanotechnology. The authors also acknowledge members of the MSKCC Radiochemistry and Molecular Imaging Probe Core and the Alan and Sandra Gerry Metastasis and Tumor Ecosystems Center of MSKCC. We also would like to acknowledge Komal Mandleywala for her help in the preparation of spheroid slides for immunocytochemistry.

References

1. R. A. Pires, Y. M. Abul-Haija, R. L. Reis, R. V. Ulijn and I. Pashkuleva, in *Hydrogels: Design, Synthesis and Application in Drug Delivery and Regenerative Medicine*, eds. T. R. R. Singh, G. Laverty and R. Donnelly, CRC Press, 2018, ch. 10, pp. 170-183.
2. B. J. Kim and B. Xu, *Bioconjugate Chem*, 2020, **31**, 492-500.
3. C. F. Anderson and H. G. Cui, *Ind Eng Chem Res*, 2017, **56**, 5761-5777.
4. R. A. Pires, Y. M. Abul-Haija, D. S. Costa, R. Novoa-Carballal, R. L. Reis, R. V. Ulijn and I. Pashkuleva, *J Am Chem Soc*, 2015, **137**, 576-579.
5. J. Zhou and B. Xu, *Bioconjugate Chem*, 2015, **26**, 987-999.
6. H. M. Wang, Z. Q. Q. Feng and B. Xu, *Chem Soc Rev*, 2017, **46**, 2421-2436.
7. J. Li, D. Bullara, X. Du, H. He, S. Sofou, I. G. Kevrekidis, I. R. Epstein and B. Xu, *ACS Nano*, 2018, **12**, 3804-3815.
8. J. Zhou, X. Du, N. Yamagata and B. Xu, *J Am Chem Soc*, 2016, **138**, 3813-3823.
9. Z. Q. Zhou, X. Xie, Q. K. Yi, W. C. Yin, A. A. Kadi, J. B. Li and Y. Zhang, *Org Biomol Chem*, 2017, **15**, 6892-6895.
10. K. Duval, H. Grover, L. H. Han, Y. Mou, A. F. Pegoraro, J. Fredberg and Z. Chen, *Physiology*, 2017, **32**, 266-277.
11. P. M. R. Pereira, N. Berisha, N. Bhupathiraju, R. Fernandes, J. P. C. Tome and C. M. Drain, *Plos One*, 2017, **12**.
12. A. Brito, P. M. R. Pereira, D. Soares da Costa, R. L. Reis, R. V. Ulijn, J. S. Lewis, R. A. Pires and I. Pashkuleva, *Chem Sci*, 2020, **11**, 3737-3744.
13. J. Barretina, G. Caponigro, N. Stransky, K. Venkatesan, A. A. Margolin, S. Kim, C. J. Wilson, J. Lehar, G. V. Kryukov, D. Sonkin, A. Reddy, M. W. Liu, L. Murray, M. F. Berger, J. E. Monahan, P. Morais, J. Meltzer, A. Korejwa, J. Jane-Valbuena, F. A. Mapa, J. Thibault, E. Bric-Furlong, P. Raman, A. Shipway, I. H. Engels, J. Cheng, G. Y. K. Yu, J. J. Yu, P. Aspesi, M. de Silva, K. Jagtap, M. D. Jones, L. Wang, C. Hatton, E. Palescandolo, S. Gupta, S. Mahan, C. Sougnez, R. C. Onofrio, T. Liefeld, L. MacConaill, W. Winckler, M. Reich, N. X. Li, J. P. Mesirov, S. B. Gabriel, G. Getz,

K. Ardlie, V. Chan, V. E. Myer, B. L. Weber, J. Porter, M. Warmuth, P. Finan, J. L. Harris, M. Meyerson, T. R. Golub, M. P. Morrissey, W. R. Sellers, R. Schlegel and L. A. Garraway, *Nature*, 2012, **483**, 603-607.

14. Z. C. Nwosu, M. P. Ebert, S. Dooley and C. Meyer, *Mol Cancer*, 2016, **15**, 71.
15. R. G. W. Anderson, *Annu Rev Biochem*, 1998, **67**, 199-225.
16. A. Fasano, in *New Challenges for Cancer Systems Biomedicine*, eds. A. Donofrio, P. Cerrai and A. Gandolfi, 2012, vol. 1, pp. 173-190.
17. E. Warnke, J. Pietsch, M. Wehland, J. Bauer, M. Infanger, M. Gorog, R. Hemmersbach, M. Braun, X. Ma, J. Sahana and D. Grimm, *Cell Commun Signaling*, 2014, **12**, 32.
18. T. Amann, U. Maegdefrau, A. Hartmann, A. Agaimy, J. Marienhagen, T. S. Weiss, O. Stoeltzing, C. Warnecke, J. Scholmerich, P. J. Oefner, M. Kreutz, A. K. Bosserhoff and C. Hellerbrand, *Am J Pathol*, 2009, **174**, 1544-1552.
19. R. C. Osthus, H. Shim, S. Kim, Q. Li, R. Reddy, M. Mukherjee, Y. Xu, D. Wonsey, L. A. Lee and C. V. Dang, *J Biol Chem*, 2000, **275**, 21797-21800.
20. P. Longati, X. H. Jia, J. Eimer, A. Wagman, M. R. Witt, S. Rehnmark, C. Verbeke, R. Toftgard, M. Lohr and R. L. Heuchel, *Bmc Cancer*, 2013, **13,** 95.
21. D. A. Chan, P. D. Sutphin, P. Nguyen, S. Turcotte, E. W. Lai, A. Banh, G. E. Reynolds, J. T. Chi, J. Wu, D. E. Solow-Cordero, M. Bonnet, J. U. Flanagan, D. M. Bouley, E. E. Graves, W. A. Denny, M. P. Hay and A. J. Giaccia, *Sci Transl Med*, 2011, **3**, 94ra70.
22. C. Granchi, S. Fortunato and F. Minutolo, *Medchemcomm*, 2016, **7**, 1716-1729.
23. N. Hay, *Nat Rev Cancer*, 2016, **16**, 635-649.
24. P. P. Hsu and D. M. Sabatini, *Cell*, 2008, **134**, 703-707.
25. M. G. V. Heiden, L. C. Cantley and C. B. Thompson, *Science*, 2009, **324**, 1029-1033.
26. Y. Kuang, J. F. Shi, J. Li, D. Yuan, K. A. Alberti, Q. B. Xu and B. Xu, *Angew Chem Int Edit*, 2014, **53**, 8104-8107.
27. F. K. Chan, K. Moriwaki and M. J. De Rosa, *Methods Mol Biol*, 2013, **979**, 65-70.
28. J. Gamrekelashvili, C. Kruger, R. von Wasielewski, M. Hoffmann, K. M. Huster, D. H. Busch, M. P. Manns, F. Korangy and T. F. Greten, *J Immunol*, 2007, **178**, 1573-1580.
29. P. M. R. Pereira, S. K. Sharma, L. M. Carter, K. J. Edwards, J. Pourat, A. Ragupathi, Y. Y. Janjigian, J. C. Durack and J. S. Lewis, *Nat Commun*, 2018, **9**, 5137.

SUPPLEMENTARY INFORMATION

Aromatic carbohydrate amphiphile disrupts cancer spheroids and prevents relapse

Alexandra Brito,[a-d] Patrícia M. R. Pereira,[c] Rui L. Reis,[a,b] Rein V. Ulijn,[d-f] Jason S. Lewis,[c,g-j] Ricardo A. Pires,*[a,b] and Iva Pashkuleva*[a,b]

[a]3B's Research Group, I3Bs - Research Institute on Biomaterials, Biodegradables and Biomimetics, University of Minho, Headquarters of the European Institute of Excellence on Tissue Engineering and Regenerative Medicine, AvePark, Parque de Ciência e Tecnologia, Zona Industrial da Gandra, 4805-017 Barco, Guimarães, Portugal; [b]ICVS/3Bs - PT Government Associate Laboratory, Braga/Guimarães, Portugal; [c]Department of Radiology, Memorial Sloan Kettering Cancer Center; [d]Advanced Science Research Center (ASRC) at the Graduate Center, City University of New York (CUNY), 85 St Nicholas Terrace, New York, New York 10031, USA; [e]Department of Chemistry, Hunter College, City University of New York, 695 Park Avenue, New York 10065, USA; [f]PhD programs in Biochemistry and Chemistry, The Graduate Center of the City University of New York, New York 10016, USA; [g]Department of Radiology, Weill Cornell Medical College, New York, NY 10065, USA; [h]Molecular Pharmacology Program, Memorial Sloan Kettering Cancer Center, New York, NY 10065, USA; [i]Department of Pharmacology, Weill Cornell Medical College, New York, NY 10065, USA; [j]Radiochemistry and Molecular Imaging Probes Core, Memorial Sloan Kettering Cancer Center, New York, NY 10065, USA

Materials and Methods

*Synthesis and purification of N-fluorenylmethyloxycarbonyl-glucosamine-6-phosphate (**1**).*

The compound **1** was obtained from the respective glucosamine-6-phosphate using our previously described one-step procedure.[1-3] Briefly, the sodium salt of the glucosamine-6-phosphate was dissolved in water (30 g/L) in the presence of 2 eq sodium hydrogen carbonate (Riedel-de Haen, Germany) and reacted with 1.5-2 eq 9-fluorenylmethoxycarbonyl chloride (Fmoc-Cl, Sigma, Germany) dissolved in dioxane until complete consumption of the carbohydrate (detected by TLC). The product was purified by column chromatography (230-400 mesh silica gel) to remove the non-reacted Fmoc (eluent EtOAc:MeOH:H_2O, 5:3:2). The purity of the compound was confirmed by HPLC, MS, and NMR.

Monolayer (2D) cell cultures

SaOs2 osteosarcoma cells, MCF-7 and HS578T breast cancer cells were obtained from the American Type Culture Collection (ATCC, Manassas, VA, USA). SaOs2 and HS578T cells were cultured in Dulbecco´s Modified Eagle´s Medium (DMEM, Sigma or MSKCC media preparation core). MCF-7 cells were cultured in Eagle´s Minimum Essential Medium (EMEM; Corning, NY, USA or MSKCC media preparation core) with 1.5 g/L sodium bicarbonate, non-essential amino acids, L-glutamine and sodium pyruvate. Both culture media were supplemented with 10% (v/v) of fetal bovine serum (Life Technologies, Carlsbad, CA, USA), 100 U/mL penicillin, 100 µg/mL streptomycin and 0.25 µg/mL amphotericin B (Sigma). The cultures were maintained at 37°C in a 5% CO_2 humidified atmosphere.

Spheroids formation and characterization

Spheroids were generated by growing cancer cell suspensions in agarose-coated 96 well plates.[4] The agarose prevented the cells from attaching to the bottom of the wells. Briefly, 150 µl/well of 1.5% (w/v in PBS) agarose solution (MP Biomedicals, Santa Ana, CA, USA) was added to the wells of a 96-well microplate. Cells (SaOs2, MCF-7 or HS578T with densities ranging from 2,500 to 20,000 cells per well) were then added and the microplate was hand-spun gently. Clusters of cancer cells were observed after 24 h of seeding, except for SaOs2 cells. Within the following 24 h the clusters formed spheroids for the HS578T cells, *i.e.* stable round aggregates which are not dislodged by pipetting. Images of clusters/aggregates/spheroids were obtained at 24, 48 and 72 h after cell culturing using the image analysis system consisting of Nikon Eclipse Ti fluorescent microscope and an Andor iXon EMCCD camera. The size of at least 6 spheroids was calculated for each cell line by measuring two orthogonal diameters (d1 and d2) using the line morphometry function. Volumes were calculated using equation 1:

$$\text{Volume} = \frac{4}{3}\pi r^3 \qquad \text{equation 1}$$

where $r = \frac{1}{2} \times (d1 + d2)$ is the geometric mean radius. Average cell number per spheroid was also determined

at 24, 48 and 72 h after cell culturing by trypsinizing six different spheroids, mixing the cell suspension with Trypan blue (Sigma) and counting the number of total and viable cells, using a Vi-CELL XR, Cell Counter - Beckman Coulter.

*Treatment of spheroids and 2D flat cultures with **1***

Monolayers and spheroids cultures were supplemented with 0.5 mM or 1 mM of compound **1**, dissolved in media specifc for each cell line. The supplemented cultures were maintained for 24, 48 or 72 h and then analyzed as described below.

Lactate dehydrogenase (LDH) assays

The cytotoxicity of **1** was assessed using the CytoTox 96H Non-Radioactive cytotoxicity assay kit (Promega, USA) according to the manufacturer's instructions. Unlike other studies reporting the use of MTT for quantification spheroid viability, we were not able to apply this assay because the results were neither reproducible nor consistent (data not shown). Therefore, we used CytoTox 96 Assay to quantify the LDH released from the spheroids as an indicator of cytotoxicity. Briefly, 50 µL of culture medium was collected from the well (96-well plate) containing cell spheroids and mixed with 50 µL of the CytoTox 96 Reagent in dark for 30 min at room temperature. Then 50 µL of stop solution was added to each well and the absorbance was recorded at 490 nm using a microplate reader (PowerWave HT Microplate Spectrophotometer). The average values of the culture medium background were subtracted from all values of experimental wells. The protein concentration was determined by Pierce BCA Protein Assay Kit after scrapping spheroid cultures in 1% (m/v) SDS solution in PBS (pH 7.0), and LDH activity was normalized to the protein concentration. The results were normalized to the maximal LDH release, which was determined by treating the control wells for 60 min with 1% Triton X-100 to lyse all cells.

Transfection assay

GLUT1 was depleted using a pool of three target-specific 19–25 nt siRNA and CAV1 with a pool of 20–25 nt siRNA (Santa Cruz Biotechnology). [4] Cancer cells were transfected with either SLC2A1-siRNA, siRNA-CAV1 or scrambled (scr) siRNA (controls). Each transfection was performed for 5 h with 2.4 µM of siRNA in transfection medium (Santa Cruz) containing 0.5 µL/cm^2 of transfection reagent (Santa Cruz). After incubation with siRNA , complete media was added and the cells were incubated for 48 h. CAV1 and GLUT1 downregulation was assessed at 24, 48 and 72 h post-transfection by Western Blotting.

ALP inhibition

For alkaline phosphatase inhibition assays, we used the Pierce phosphatase inhibitor (Thermo Scientific) according to the manufacturer instruction (1 tablet per 10 mL of culture medium with FBS).

Preparation of cell extracts and Western Blot

Scraped monolayer cells and spheroids cultured for 48 h were collected at 1,500 g for 5 min, washed twice with ice-cold PBS and whole protein lysates were extracted using RIPA buffer (150 mM NaCl, 50 mM Tris-HCl, pH 7.5, 5 mM ethylene glycol tetra-acetic acid, 1% Triton X- 100, 0.5% sodium deoxycholate, 0.1% SDS, 2 mM phenylmethanesulfonyl, 2 mM iodoaceta- mide, and 1x protease inhibitor cocktail (Roche, Indianapolis, USA)). Cell extracts were centrifuged at 16,000 g for 10 min at 4°C. After centrifugation, supernatants were used for protein quantification using the Pierce BCA Protein Assay Kit, followed by denaturation of the sample with Laemmli buffer. For the Western Blot analysis, 40 µg proteins were loaded per lane on sodium dodecyl sulphate-polyacrylamide gels (SDS-PAGE). Following electrophoresis and transfer to polyvinylidene fluoride membranes (Bio-Rad, Hercules, CA, USA), the blots were incubated in 5% (w/v) BSA in TBS-T (20 mM Tris, 150 mM NaCl, Tween 0.2%, pH 7.6). Membranes were then incubated with rabbit anti-GLUT1 1:1,000 (Thermo Fisher Scientific), rabbit anti- CAV1 1:1,000 (Thermo Fisher Scientific), rabbit anti-ALP 1:1,000 (Thermo Fisher Scientific) and rabbit anti-β-actin 1:1,000 (Thermo Fisher Scientific) antibodies. After washing, the membranes were incubated with IRDye 800CW anti-Rabbit IgG 1:15,000 (LI-COR Biosciences, Lincoln, NE, USA) and imaged on the Odyssey Infrared Imaging System (LI-COR Biosciences) followed by densitometric analysis.

Immunofluorescence microscopy

Spheroids were grown for 48 h and then treated as described above. Live-dead staining: after treatment, the spheroids were placed in a new 96 well plate without agarose and were stained with calcein AM (CA, 3 μM) and propidium iodide (PI, 3 μM) in 200 μl of phosphate-buffered saline (PBS). Imaging with a Leica TCS SP5 Confocal Laser Scanning Microscope was performed 3h after the staining. Immunolocalization: spheroids were placed in Optimal Cutting Temperature (OCT) mounting media and frozen immediately. After that, blocks were cut in sections of 10 μM. The sections were then dried at room temperature and fixed for 10 min with cold acetone. After washing with PBS, the spheroid was permeabilized with 0.25% v/v Triton X-100 in PBS with 0.02% w/v BSA in a humidified chamber and blocked with 10% v/v normal goat serum for 2h at room temperature. The spheroids were then incubated overnight at 4 °C with HIF-1α-488 (Abcam; 1:100), CAV1 (Abcam; 1:500), GLUT1 (Sigma-Aldrich, 1:100) or ALP (Abcam, 1:250). The spheroids were then rinsed with 0.02% BSA, 0.02% (w/v) sodium azide (NaN_3) in PBS. Secondary fluorescent antibody Alexa Fluor 488 (Abcam, 1:1000) was applied for 1h at room temperature, except for HIF-1α-488, which is fluorescent-labeled. The spheroids were rinsed with 0.02% (w/v) NaN_3 and were incubated with DAPI (Abcam, 1:1000) for 15 min at room temperature, followed by rinsing with 0.02% (w/v) NaN_3. The spheroids were mounted in glycergel mounting medium and were imaged using a Leica TCS SP5 Confocal Laser Scanning Microscope. Sections were also submitted to MSKCC Molecular Cytology Core Facility for hematoxylin and eosin staining. In all experiments, untreated spheroids were used as controls and manipulated following the same protocols as for the treated ones.

Fluorescence quantification

Each of the channels (green and blue) of the images obtained by immunofluorescence microscopy after staining for ALP, GLUT1 or CAV1 was converted to gray scale. To quantify the expression of each protein, we used Cell Profiler 3.0 Software. The threshold was optimized for each signal to separate it from the background and the respective maximum intensity per total area was determined. The obtained value for the green signal was divided by the blue one, *i.e.* protein signal was normalized by the number of cells. For each condition 6-10 images were analyzed.

Scanning electron microscopy

The spheroids were placed onto a silica-wafer, dried at room temperature and imaged using high-resolution scanning electron microscopy (HRSEM, Auriga Compact, ZEISS) at 5kV after coating with 1nm of platinum.

Statistical analysis

Statistical analyses were carried out using a statistical program (GraphPad Prism; GraphPad Software). Student's *t*-test was used to evaluate the effect of the treatment compared with the control. P- values were considered at the 5% level of significance to deduce inference of the significance of the data, were * $p < 0.01$; ** $p < 0.005$; *** $p < 0.001$; **** $p < 0.0001$.

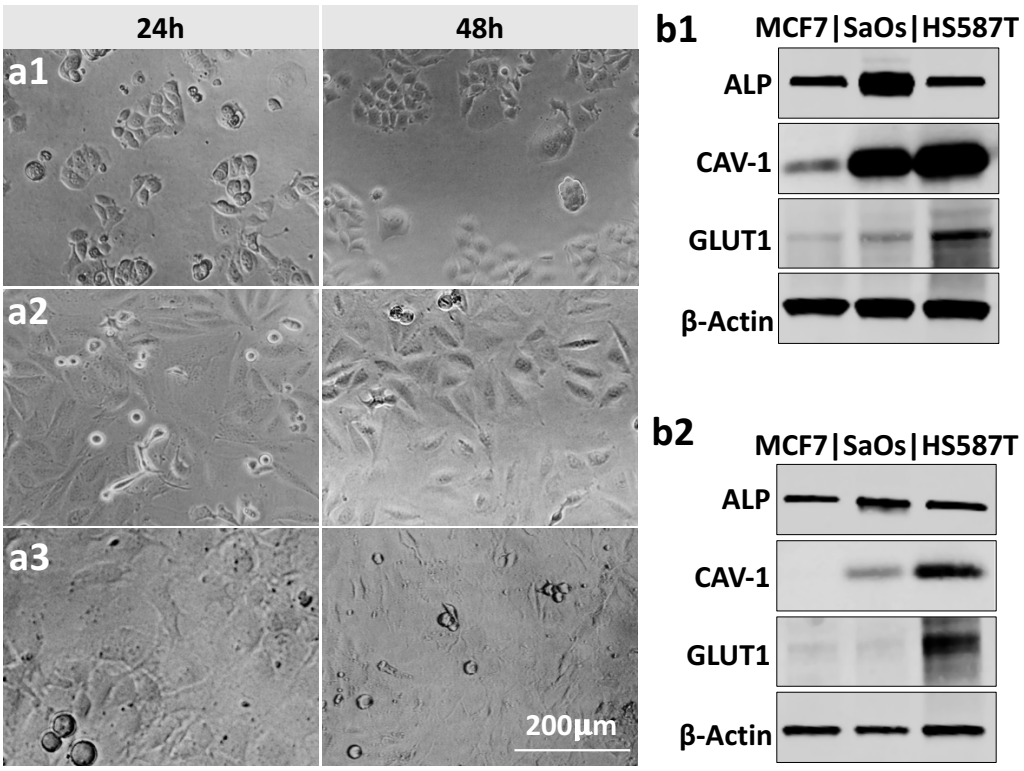

Supplementary figure S1. (a) Microscopy images of **(a1)** MCF7, **(a2)** SaOs2, and **(a3)** HS587T cells seeded on flat tissue culture plates for different time and **(b)** Western-Blot analysis of ALP, CAV-1, and GLUT1 expression by **(b1)** these cells and **(b2)** spheroids/aggreagates generated from them 48h after seeding. β-Actin was used to normalize the data in the densiometry analysis presented in Figure 1 of the main manuscript.

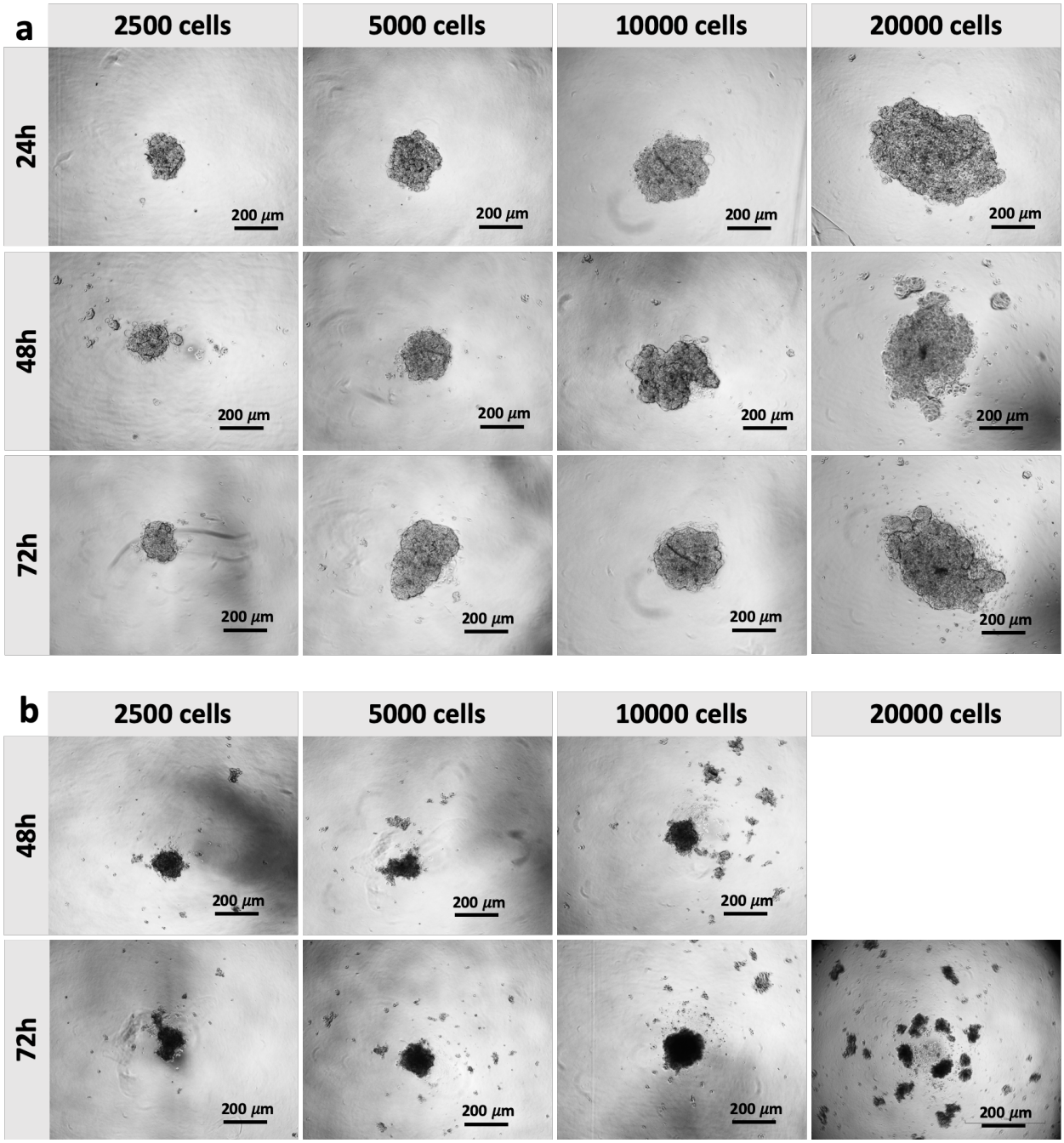

Supplementary figure S2. Ability of **(a)** MCF7 and **(b)** SaOs2 cells to form spheroids at different cell seeding desity (2,500 – 20,000 cells per well) and timeframe (24 – 72 h). No cells aggregates or spheroids were observed after 24 h for SaOs2 cells.

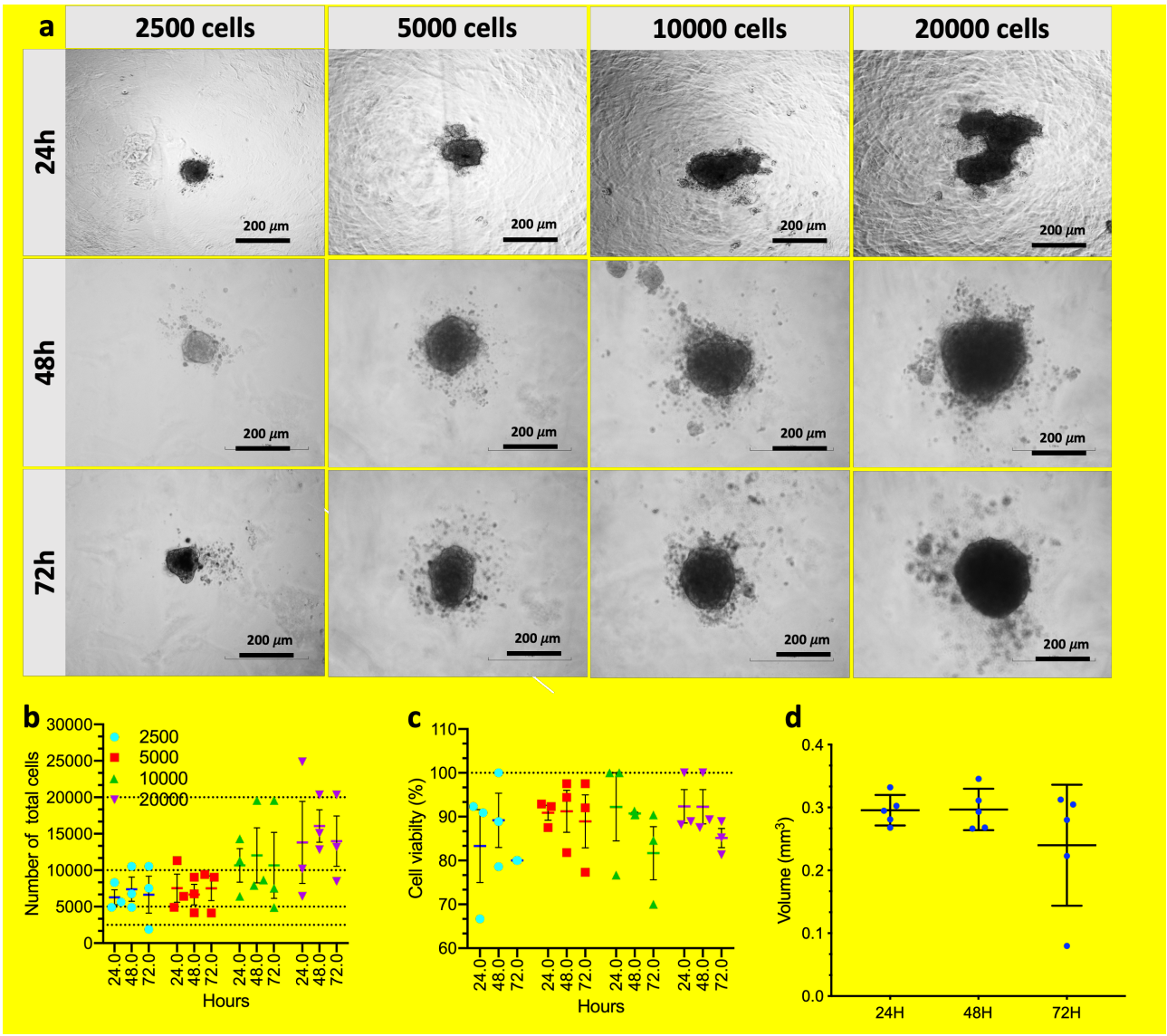

Supplementary figure S3. Effect of the conditions (seeding density and culture time) on the formation of HS578T spheroids: (**a**) representative optical microscopy images of the aggregates/spheroids; (**b**) number of total HS578T cells forming the aggregates/spheroids and (**c**) their viability (obtained from the ratio between live cells and the total number of cells within the 3D cell structure) as a function of time; (**d**) volume of the spheroids generated at a cell seeding density of 5,000 cells/well.

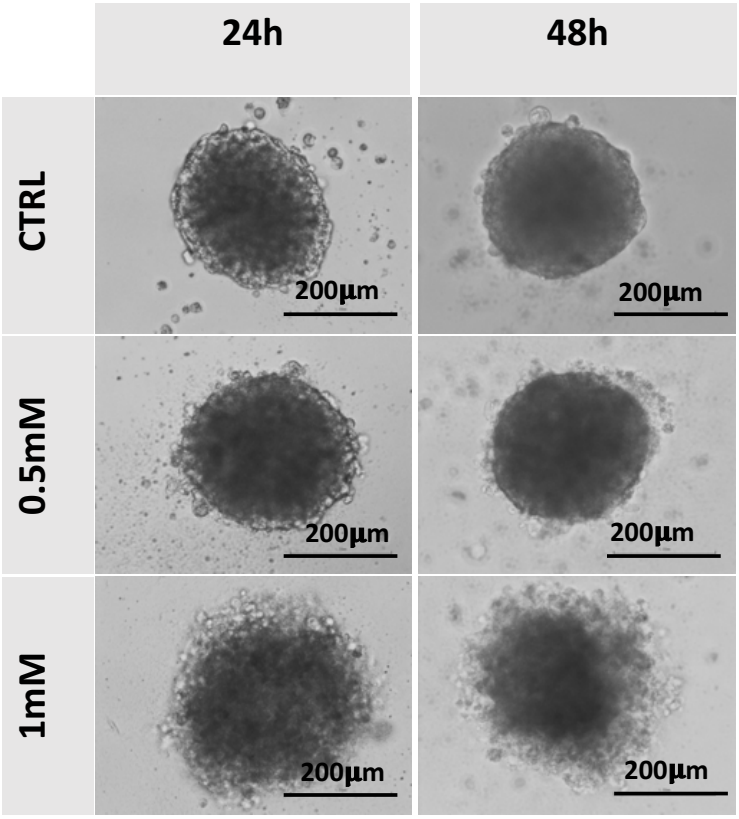

Supplementary figure S4. Light microscopy images of untreated spheroids (control, CTRL) and spheroids exposed to **1** at different concentration (0.5 and 1 mM) and for different timeframe (24 and 48 h).

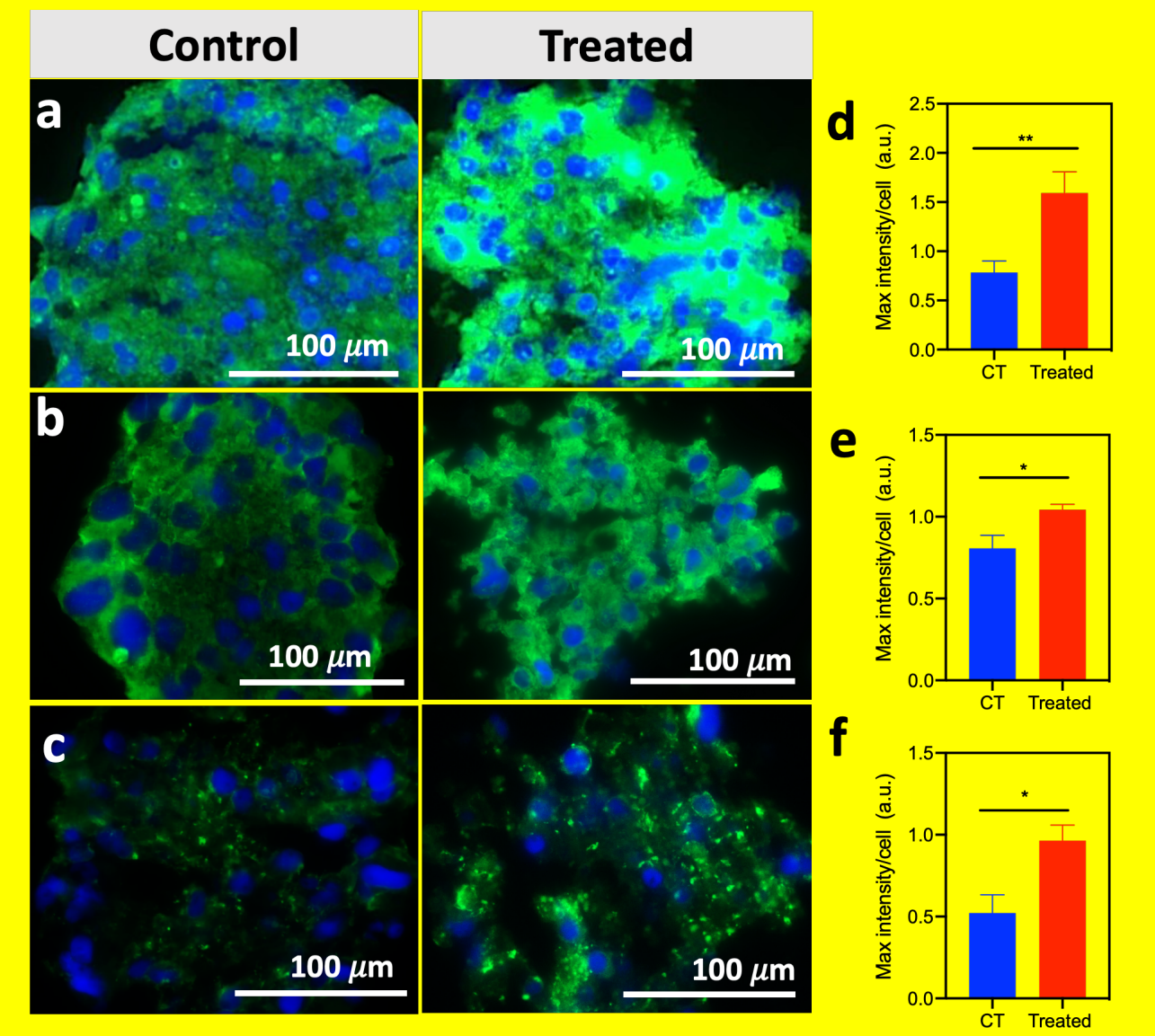

Supplementary figure S5. Immunolocalization of (**a**) ALP, (**b**) GLUT1, and (**c**) CAV1 showed by confocal microscopy images of untreated spheroids (control) and spheroids exposed to **1** (1 mM, 48 h). Expression of (**d**) ALP, (**e**) GLUT1, and (**f**) CAV1 obtained by quantification of the fluorescence using Cell Profiler 3.0 Software. Statistical data were obtained using t-test $^{**}p < 0.01$; $^{*}p < 0.05$.

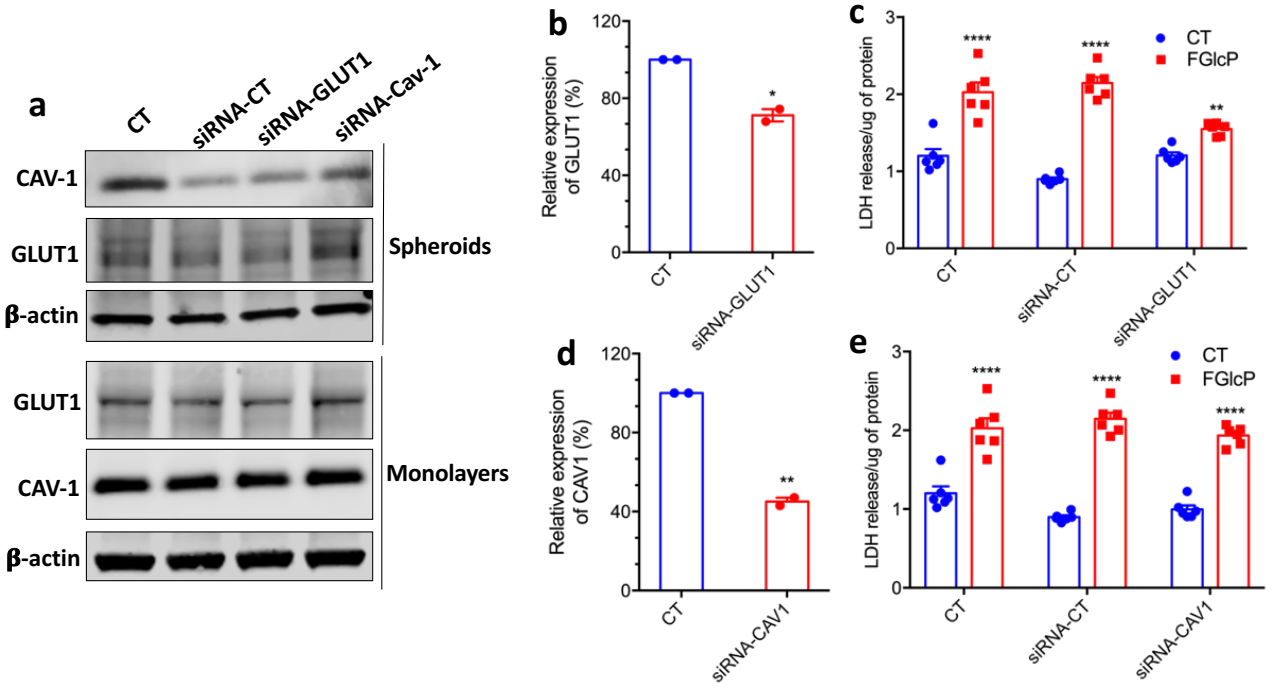

Supplementary figure S6. (**a**) Western Blot analysis and respective densitometry analysis showing the relative expression of (**b**) GLUT1 and (**d**) CAV1 in HS587T spheroids after depletion of the respective genes. Controls (CT) for the data presented on Figure 3 in the main manuscript: effect of (**c**) GLUT1 and (**e**) CAV1 knockout on the cell viability determined by LDH release. siRNA-CT is abbreviation used for non-specific siRNA.

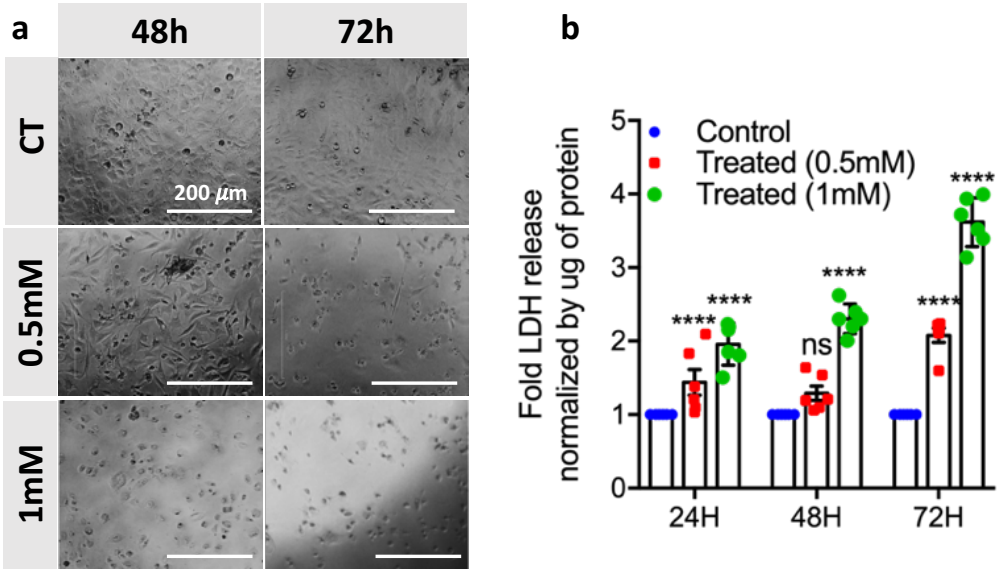

Supplementary figure S7. (**a**) Representative images of the monolayers of HS578T cells supplemented with **1** (0 - 1mM) for different time (48-72h) and the respective (**b**) cell viability indicated by LDH release; * $p < 0.01$; ** $p < 0.005$; *** $p < 0.001$; **** $p < 0.0001$.

Q3. In theory, Figure 2a, Figure 4a1, Figure S3 (5000 cells, 48 h), and Figure S4 (control, 48 h) are all 3D cell spheres under the same conditions. Why do they (the control group) look very different?
A3: To facilitate the reading/understanding, we uniform the presentation of the figures/scale bars and modified the figures captions to include the specific microscopy setting used to obtain these images. Spheroids on Figure 4 are different as they were removed from agarose-coated plates and then re-plated in adherent well plates as described in the experimental section.

Q4. *In the figures, some dots have no indications. For example, the black dots in Figure 1c; the purple dots in Figure 3 (c, d, e); the blue dots in Figure S3.*
A4: The points represent the whole data set obtained for each condition (so-called dot or scatter plots) and used to calculate the descriptive statistics elements, *i.e.* data distribution, average values and standard deviations. This representation is recommended because is more informative as compared with simple bar charts and box plots [J Ho et al, Nature Methods 2019 16:565].

Q5. *Why does the volume of the spheroids at 72 h approach to 0 in Figure S3d?*
A5: We apologize for this mistake and corrected it in the revised manuscript.

Q6. *There are some question marks above the scale bar in the figures. This should be changed.*
A6: We have edited the figures in the revised manuscript.

Q7. *In this manuscript, the authors stated that MCF-7 cells cannot form 3D cell spheres. In fact, there are many successful examples to build 3D cell sphere models using MCF-7 cells in other literature (e.g., ACS Appl. Mater. Interfaces 2020, 12, 27, 30221–30233). The authors should look for the reasons*
A7: There are many works that use MCF7 spheroids and based on these previous references we also tested this cell line. However, the spheroids can be obtained at different conditions (*e.g.* cell density, culture time) and by different methods (*e.g.* hanging drop, spinning flask, microwell arrays) each of which has its advantages and drawbacks. For our studies, we used the agarose coating protocol and we observed that at the studied conditions MCF7 did not form reproducible spheroids. Because the aim of our study was not to assess/optimize different methods for spheroids formation, we just excluded this cell line from our experiments and used only the ones that showed reproducible results.

We are looking forward to hearing from you.

Sincerely yours,
Alexandra Brito
Patrícia Ribeiro
Rui L. Reis
Rein V. Ulijn
Jason Lewis
Ricardo A. Pires
Iva Pashkuleva